

Near-infrared Monitoring of the Accretion Outburst in the MYSO S255-NIRS3

Mizuho UCHIYAMA¹, Takuya YAMASHITA², Koichiro SUGIYAMA^{3,4}, Tatsuya NAKAOKA⁵, Miho KAWABATA^{6,7,5}, Ryosuke ITOH^{8,5}, Masayuki YAMANAKA^{6,7,5}, Hiroshi AKITAYA⁵, Koji KAWABATA⁵, Yoshinori YONEKURA⁹, Yu SAITO⁹, Kazuhito MOTOGI¹⁰ and Kenta FUJISAWA¹¹

¹Advanced Technology Center, National Astronomical Observatory of Japan (NAOJ), 2-21-1 Osawa, Mitaka, Tokyo 181-8588, Japan

²TMT-J Project Office, NAOJ, 2-21-1 Osawa, Mitaka, Tokyo 181-8588, Japan

³Mizusawa VLBI Observatory, NAOJ, 2-21-1 Osawa, Mitaka, Tokyo 181-8588, Japan

⁴National Astronomical Research Institute of Thailand, 260 Moo 4, T.Donkaew, A. Maerim, Chiang Mai, 50180, Thailand

⁵Hiroshima Astrophysical Science Center, Hiroshima University, 1-3-1 Kagamiyama, Higashi-Hiroshima, Hiroshima 739-8526, Japan

⁶Department of Astronomy, Kyoto University, Kitashirakawa-Oiwake-cho, Sakyo-ku, Kyoto 606-8502, Japan

⁷Okayama Observatory, Kyoto University, 3037-5 Honjo, Kamogata, Asakuchi, Okayama 719-0232, Japan

⁸Bisei Astronomical Observatory, 1723-70 Okura, Bisei, Ibara, Okayama 714-1411, Japan

⁹Center for Astronomy, Ibaraki University, 2-1-1 Bunkyo, Mito, Ibaraki 310-8512, Japan

¹⁰Graduate School of Sciences and Technology for Innovation, Yamaguchi University, 1677-1 Yoshida, Yamaguchi, Yamaguchi 753-8512, Japan

¹¹The Research Institute for Time Studies, Yamaguchi University, 1677-1 Yoshida, Yamaguchi, Yamaguchi 753-8511, Japan

*E-mail: mizuho.uchiyama@nao.ac.jp

Received 2019 June 19; Accepted 2019 October 16

Abstract

We followed-up the massive young stellar object (MYSO) S255-NIRS3 (=S255-IRS1b) during its recent accretion outburst event in the *Ks* band with Kanata/HONIR for four years after its burst and obtained a long-term light curve. This is the most complete NIR light-curve of the S255-NIRS3 burst event that has ever been presented. The light curve showed a steep increase reaching a peak flux that was 3.4 mag brighter than the quiescent phase and then a relatively moderate year-scale fading until the last observation, similar to that of the accretion burst events such as EXors found in lower-mass young stellar objects. The behavior of the *Ks* band light curve is similar to that observed in 6.7 GHz class II methanol maser emission, with a sudden increase followed by moderate year-scale fading. However, the maser emission peaks appear 30-50 days earlier than that of the *Ks* band emission. The similarities confirmed that the origins of the maser emission and the *Ks* band continuum emission is common as previously shown from another infrared and radio observations by Stecklum et al. (2016); Caratti o Garatti et al. (2017a); Moscadelli et al. (2017). However, the differences in energy transfer paths, such as the exciting/emitting/scattering structures, may cause the delay in the flux-peak

dates.

Key words: stars: formation — stars: individual (S255-NIRS3) — stars: massive — stars: variables: general

1 Introduction

Massive stars play an important role in the galaxies and cosmic evolution. Their feedbacks, such as supernova explosions and stellar winds, affect the surrounding environment significantly (Tan et al. 2014; Zinnecker & Yorke 2007). However, detailed mass-growth processes of massive young stellar objects (MYSOs) were not clear until now. Three major candidate processes—core accretion, competitive accretion, and stellar collision—have been proposed but it is still not clear which process is the dominant one although stellar collision might be efficient only in an extremely crowded region and might not be a frequent process (Tan et al. 2014). Because the formation of massive stars is deeply obscured by dense gas and dust, and is located relatively far from us (typically farther than 1 kpc), their physical structure is hard to resolve. In fact, currently available spatial resolution of observations is insufficient to resolve inner 10AU-scale structures of the MYSOs and their disks, where the mass growth phenomenon happens, unless VLBI technique are used (Tan et al. 2014). VLBI observations, however, mostly detect only non-thermal emissions such as masers, and it is difficult to investigate the physical parameters and structures of the emitting regions. Therefore, other observational methods are required to observe the inner structures in more detail.

Variability study is a promising method for this purpose. Such studies of low-mass young stellar objects at optical and infrared wavelengths have proven to be powerful tools for deciphering the physics of star formation and pre-main-sequence stellar evolution, such as stellar rotation, the existence and characteristics of cool/hot spots, infalling/rotating dusty objects, and the variation in accretion rate (Morales-Calderón et al. 2011).

Although the peak of spectral energy distribution in MYSOs is located in the mid-infrared (MIR) or the far-infrared (FIR), near-infrared (NIR) observations are suitable for long-term and/or high-cadence monitoring owing to accessibility of the available facilities. One pioneering study reported the observation of seven reflection nebulae of Cep A East in the K_s band for several years and showed the variability of all the components (Hodapp & Bressert 2009). The authors suggested that the variability should be caused by the variation in dust extinction caused by a rotating structure around ~ 10 AU from the MYSO (Hodapp & Bressert 2009). Recently, 13 high amplitude ($\Delta K > 1$ mag) year-scale variable MYSOs in the K_s band were reported for the first time using VVV survey data (Kumar et al. 2016) and another work also detected 190 lower-amplitude variable MYSOs out of 718 samples (Teixeira et al. 2018). These

studies imply that variability is common in MYSOs also and have the potential to reveal the physical processes happening in the inner regions of MYSOs. Higher-cadence observations of these variable MYSOs are required to get more details of their physical structure and the phenomena happening much inside the MYSOs and/or their surrounding disks. In addition to such observations, NIR follow-up observations of possible drastic changes in the physical conditions of such MYSOs, such as sudden increase in radio fluxes, are also important to study their nature.

Among the origins of variability, accretion burst events are well-known events causing drastic variability in low-mass young stellar objects (YSOs) (Audard et al. 2014, and references therein). Recently, their appearance was theoretically proposed in MYSOs as well (Meyer et al. 2017) and observed for the first time in S255-NIRS3 at infrared wavelengths (Caratti o Garatti et al. 2017a). Later on, another accretion burst in an MYSO (NGC 6334I-MM1) was detected at sub-mm wavelengths (Hunter et al. 2017). In addition, the radio jet burst triggered by the accretion burst was also detected in S255-NIRS3 (Cesaroni et al. 2018).

In October 2015, a class II methanol maser outburst at 6.7 GHz was reported in S255 region (Fujisawa et al. 2015). This discovery triggered a search for the exciting source. Because a class II methanol maser is expected to be associated with the thermal emission of dust in disks (Norris et al. 1993; Minier et al. 2000; Cragg et al. 2005; Bartkiewicz et al. 2009; Sugiyama et al. 2014), origins of the maser outburst would be very close to the MYSO, and flux variation in the infrared would also be expected. Stecklum et al. (2016) identified S255 NIRS3, with a trigonometric distance of 1.78 kpc (Burns et al. 2016), as the exciting source suggesting, for the first time, the possibility of an accretion outburst in a massive YSO and its connection with the maser flare. Based on their infrared imaging and spectroscopic study, Caratti o Garatti et al. (2017a) indicated that this event was triggered by an accretion burst due to a five-fold increase in the luminosity and intensity of emission lines related to mass accretion and this was confirmed by following VLBI observations by Moscadelli et al. (2017).

Note that in some previous NIR imaging studies of the S255 region (Ojha et al. 2011), the authors named this object as S255-IRS1b, referred from Howard et al. (1997), while some NIR and radio observational works released after the burst detection (Caratti o Garatti et al. 2017a; Moscadelli et al. 2017; Cesaroni et al. 2018) named it as S255-NIRS3, referred from Tamura

et al. (1991). In this work, we refer to this MYSO as S255-NIRS3.

The previous NIR observations by Stecklum et al. (2016) and Caratti o Garatti et al. (2017a) clearly showed the drastic flux increase in S255-NIRS3. However, they only reported two monitoring observations and the NIR peak flux of the S255-NIRS3 during the maser burst was missing. Furthermore, their monitoring duration was approximately six months and a whole picture of long-term variability behavior of S255-NIRS3 was not clear in the NIR. In this study, we present the first *Ks* band photometric follow-up observations of the accretion burst and analyze the NIR light-curve trend with respect to the methanol maser light-curves at several major velocities. We conducted high-cadence imaging monitoring of S255-NIRS3 in the *Ks* band and made a detailed light curve for as long as four years, clearly showing week- to year-scale variability and the flux peak after the maser outburst event. We also compare our result with high-cadence observations of the 6.7 GHz methanol maser light-curve from other studies (Szymczak et al. 2018, Sugiyama et al. in prep.) and discuss their relationship.

2 Observations

2.1 NIR monitoring

Monitoring observations in the NIR were conducted with HONIR installed on the 1.5 m Kanata telescope located at the Higashi-Hiroshima Observatory in Japan. Although HONIR can perform simultaneous optical and NIR observations, only NIR imaging data were used in this work owing to invisibility of the object in the optical. HONIR has an infrared detector of Virgo-2K with a pixel scale of 0.295 arcsec/pix and a field of view of approximately 10 arcminutes square. A detailed performance of HONIR was reported in Akitaya et al. (2014). Monitoring observations were conducted in the *Ks* band on 31 nights from November 29, 2015 to March 27, 2019 with blank periods in the spring and summer of 2016, 2017, and 2018. Exposure time of each observation is 20 seconds and five-point-dithering are performed on each observing date. A world coordinate system was defined using registration of field stars and the coordinate of the burst object in the *Ks* band ($06^{\text{h}}12^{\text{m}}54.^{\text{s}}09$, $+17^{\circ}59'23''.1$) corresponded to that of S255-NIRS3 ($06^{\text{h}}12^{\text{m}}54.^{\text{s}}020$, $+17^{\circ}59'23''.07$; Stecklum et al. (2016)) within average seeing size of 2.5 arcsec during the whole observations. Observations in the *H* band were also performed. A diffuse and faint object is detected at coordinates of S255-NIRS3 (See Figure 1 Bottom). However, relatively bad seeing as compared to the previous NIR observations (Stecklum et al. 2016; Caratti o Garatti et al. 2017a) and contamination from surrounding nebulae made it hard to perform PSF fitting photometry and light-curve in the *H* band is not available in this work.

2.2 Data reduction and photometry

Basic data reduction was conducted with a standard reduction pipeline of HONIR based on the IRAF package. We performed point spread function (PSF) fitting photometry using the DAOPHOT package in the IRAF package. Note that we did not use data with relatively bad seeing, Full Width Half Maximum of PSF larger than 3 arcsec, to improve photometric accuracy.

We also picked the most stable pair of stars in the field with the following method. First, we measured the ADU counts of all the stars in the field whose counts were larger than a tenth of that of S255-NIRS3 with the same PSF fitting photometry method. Second, pairs of stars were made among all the counted stars and a count ratio of each pair was derived during the whole observation period; and finally, the most stable pair among them, whose count ratio showed a RMS variation of just 5.9 percent, equal to 0.062 magnitudes (See Figure 2 and Table 2), throughout the whole monitoring program, were picked as the reference stars. The fluxes of S255-NIRS3 were derived and calibrated by comparing them with the brighter star in the stable pair, 2MASS J06125939+1757214 (*J*=10.6 mag, *H*=10.1 mag, *K*=9.9 mag), whose magnitudes are taken from the 2MASS catalog (Skrutskie et al. 2006). We also derived photometric error during each night from standard deviation of magnitudes of the fainter star in the stable pair among five dithering images. An average value of deviation is 0.08 mag throughout the monitoring. Therefore average of relative photometric error in this study is 0.1 mag.

Because reference stars are YSOs, we estimated the stability of absolute magnitude. The *Ks* band magnitude of the fainter star in the stable pair, 2MASS J06125160+1758015, is 10.9 mag in the 2MASS catalog (Skrutskie et al. 2006), while that calibrated from the magnitude of 2MASS J06125939+1757214 is 10.8 mag on average. The difference of 0.1 mag should come from long-term variability of the two reference stars and we use this difference as an absolute magnitude error in this study. We summarized our photometric results in Table 2 in Appendix.

3 Results

Figures 1 (Top and middle parts) and 2 show the observed image around S255-NIRS3 and the derived light curve of S255-NIRS3 in the *Ks* band. In our observations, no new infrared sources were detected as compared with the UKIDSS archival images in 2009 (Caratti o Garatti et al. 2017a). Hence, S255-NIRS3 itself got brighter. Moreover, the surrounding nebulae also got brighter and this confirmed that the same origin made this whole flux increase, as shown from the previous NIR observations and light echo study in Caratti o Garatti et al. (2017a).

Our observations gave a detailed light curve of S255-NIRS3 in the NIR after the maser burst event with the highest cadence and the longest term. An average 1σ error of magnitudes

throughout the observations, including relative and absolute errors, are ~ 0.2 mag as described in the previous section. We derived a magnitude value of 8.7 mag in the K_s band on November 29, 2015 (UT), which is almost consistent with that of 8.9 mag on November 28 (UT) reported by Stecklum et al. (2016). The slight difference (~ 0.2 mag) between the two epochs (28 and 29 November 2015) might be due to a larger uncertainty in the presented data or by the fact that the light-curve was steeply rising. During the whole monitoring period, flux variation as large as 3.7 mag was detected (see Figure 2).

4 Discussion

4.1 Characteristics of NIR variability of S255-NIRS3

As seen in Figure 2, on the first date of observation, the magnitude of S255-NIRS3 was 8.7 mag, which is 2.7 mag brighter than that in its pre-burst phase obtained from the UKIDSS archival images in December 2009 (MJD ~ 55173) (Caratti o Garatti et al. 2017a). The light curve showed a flux increase of approximately 0.7 mag until the beginning of December 2015 (MJD = 57368.591036), and then a relatively moderate fading of 3.7 mag until the last observation on March 27, 2019 (MJD = 58569.441348). The magnitude at the last observation, 11.7 mag, became slightly below that at the quiescent phase, 11.4 mag. This may be due to a larger uncertainty in the presented data or long-term variability of S255-NIRS3. Additionally, week-by-week small-scale up-and-down flux variations were detected throughout the observations within the large-scale flux variation trend. The drastic increase in flux further confirmed that S255-NIRS3 experienced an accretion burst event as previously indicated in Caratti o Garatti et al. (2017a). In Caratti o Garatti et al. (2017a, 2017b), the authors claimed that the accretion event of S255-NIRS3 resembles EXor objects, low-mass YSOs possibly experiencing accretion burst events ($\Delta V \sim 2-3$ mag), but not so drastic as FUor objects ($\Delta V > 5$ mag) (Audard et al. 2014), with its increase of bolometric luminosity. They also shown the obtained NIR spectra of S255-NIRS3 resembles EXor objects. Another characteristic of EXor objects is the relatively short length of burst, typically a few years, while the length is generally longer than 10 years in FUor objects (Audard et al. 2014). In this study, the length of the burst is measured as about 2.5 years and this provides the last piece of evidence for confirming that the accretion burst in S255-NIRS3 is the first EXor-like accretion outburst observed in a MYSO.

While EXor objects frequently show the recurrence of a drastic flux increase (Audard et al. 2014), the monitoring observations at any wavelengths spanned only 4.5 years and only one event was detected in S255-NIRS3. Further continuous of monitoring is essentially needed for searching the recurrence of the accretion burst in S255-NIRS3.

4.2 Comparison of flux variation in S255-NIRS3 between maser and NIR

Figure 3 compares the flux variation of major velocity components of the 6.7 GHz class II methanol maser (Sugiyama et al. in prep.) and the K_s band continuum emission. Observations of the methanol maser were conducted at least daily during the whole NIR monitoring period. Sudden increase in flux and its following moderate fading are also clearly seen in the light curves of the most and the next brightest maser velocity components (6.42 and 5.83 km/s). The same trend in the maser variability was also reported in a previous radio monitoring work of Szymczak et al. (2018). Table 1 summarizes the properties of flux variations in both the maser and NIR emissions. Maser decay timescales are consistent with those seen in Figure 4 in Szymczak et al. (2018). Note that maser emission is a stimulated emission and its magnification and timescale are not proportional to the change in physical conditions, such as radiation intensity or temperature of pumping. As shown in Figure 3 and Table 1, there are some similarities in the maser and NIR emissions: 1) the magnification of flux is large (larger than 10), and 2) the decrease in flux to the stable state is relatively slow (longer than two years). These similarities indicate that the same origin, such as an accretion burst, causes the observed flux variations in both the NIR and the maser as previously indicated in Moscadelli et al. (2017). The 6.7 GHz class II methanol maser is considered to be pumped up by mid-infrared emission from warm dusty disks at a temperature of about $\sim 120-300$ K associated with MYSOs (Cragg et al. 2005; Sugiyama et al. 2014). As per this hypothesis, when an accretion burst happens, maser luminosity should increase because the increase of stellar radiation warms up the dusty surrounding disk. Note that the maser emission is stimulated emission and almost all the outbursting maser components have been still unsaturated (Moscadelli et al. 2017), providing the condition that it does not simply linearly correlate with the stellar emission. Our observed trend also confirms this situation and therefore further supports the hypothesis that MIR emission from the disk pumped up the maser emission. The same suggestion was reported in a recent study with VLBI observations of the pre- and outburst phase of S255-NIRS3 (Moscadelli et al. 2017). The study demonstrated that spatial locations of maser spots at the post-burst phase spread more widely than those at the pre-burst phase. Together with our NIR observation results, we made a sketch of the S255-NIRS3 referring their work and image as illustrated in Figure 4. This expansion suggests that increased radiation heats the disk and maser-pumping region expands toward the outside of the disk (Moscadelli et al. 2017).

However, the peak flux observation date was 30-50 days earlier in the maser than that in the NIR, and also different among major velocity components of masers, as shown in the Table. 1. This time delay cannot be simply explained by the

above mechanism, in which stellar radiation causes the increment of disk thermal emission. However, assuming that the central NIR emission is scattered light as mentioned in Caratti o Garatti et al. (2017a), geometrical configuration of the scattered NIR emission may explain this delay. The observed locations of S255-NIRS3 and maser emitting regions are displaced (Stecklum et al. 2016; Moscadelli et al. 2017) by < 0.1 arc-sec, which corresponds to less than 180 AU in the plane of sky at the distance of 1.8 kpc. This is approximately 1 light days, shorter than the observed delay of about 40 days, as shown in the Figure. 4. Inclination of the disk might extend the actual distance; actually, previous MIR interferometric observations of a dust disk and VLBI observation of maser spots show a nearly edge-on inner disk inclination (Boley et al. 2013; Moscadelli et al. 2017). Scattering at the flared disk edge or a stem of out-flow cavity might explain the situation but observational evidence is not sufficient.

NIR observations started 100 days after the maser burst. Therefore, the observed flux peak in the NIR might possibly be the second peak after the accretion burst. If this is the case, the comparison of the NIR and maser peaks does not make sense. The previous light echo analysis given by Caratti o Garatti et al. (2017a) indicated that the accretion burst occurred from middle of June 2015. If this date corresponds to the first flux peak in the NIR, time delay between NIR and maser could be about 3 or 4 months (Fujisawa et al. 2015; Caratti o Garatti et al. 2017a). However, there does not seem to exist the maser peak corresponding to the second NIR flux peak, assuming that the maser peak appears 3-4 months behind of the observed NIR flux peak (MJD ~ 57450 -57500). This hypothesis may be further examined with a multi-color light echo study of S255-NIRS3 in the future. Immediate and high-cadence follow-up observations of burst MYSOs in both the NIR and maser right after burst events are critically important to reveal the true correlation between the NIR and maser, and a possible mechanism of the time-delay between them.

Acknowledgments

This work has been supported by the Grant-in-Aid for Scientific Research (26-10274) from the JSPS.

This publication makes use of data products from the Two Micron All Sky Survey, which is a joint project of the University of Massachusetts and the Infrared Processing and Analysis Center/California Institute of Technology, funded by the National Aeronautics and Space Administration and the National Science Foundation.

IRAF is distributed by the National Optical Astronomy Observatory, which is operated by the Association of Universities for Research in Astronomy (AURA) under a cooperative agreement with the National Science Foundation.

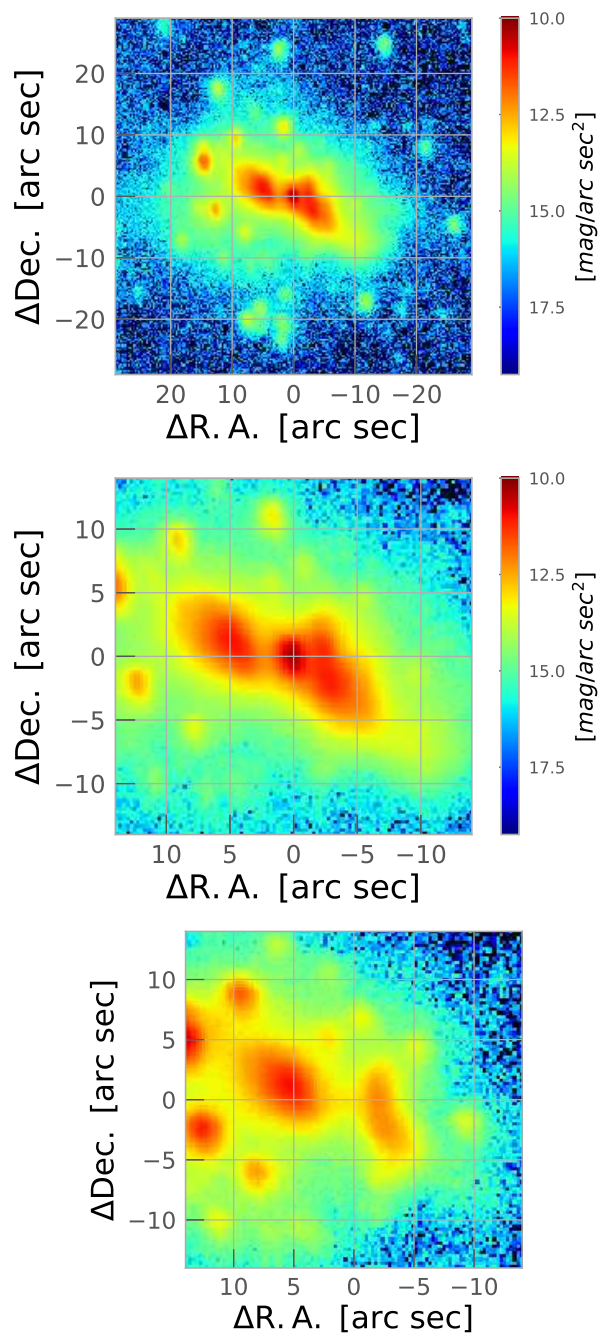


Fig. 1. (Top) Image of S255-NIRS3 region observed with Kanata/HONIR in the K_s band on December 1, 2015. (Middle) The same image but zoomed up. (Bottom) The same as middle but in the H band. The center positions are $06^h 12^m 54.^s 020$, $+17^\circ 59' 23.'' 07$ in J2000.0, corresponding to S255-NIRS3 within the seeing. The position of the known methanol maser spot is located about 0.1 arcsec east to S255-NIRS3.

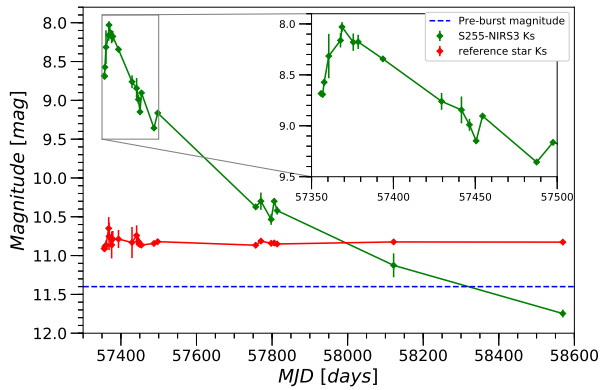


Fig. 2. A light curve of S255-NIRS3 center object in the Ks band from November 29, 2015 to March 27, 2019. A zoomed-up plot around the peak flux is also shown at the upper right part in the original plot. In these light-curves, only relative magnitude errors are presented. There also exists systematic absolute magnitude of 0.1 mag. Sudden increase of flux is clearly seen towards December 12, 2015 (MJD=57368) and the following relatively shallow fading.

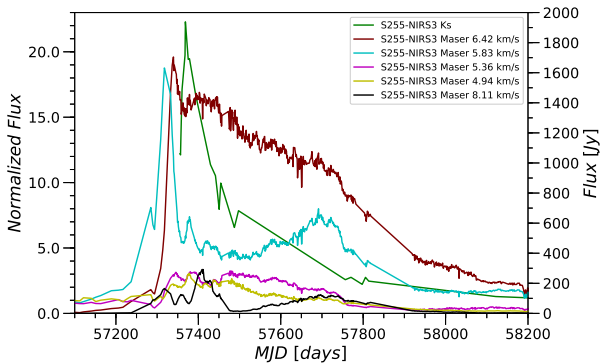


Fig. 3. Light curves of S255-NIRS3 in the Ks band and 6.7 GHz methanol maser with major velocity components. The light curve in the Ks band is normalized so that flux on the quiescent phase ($K_s = 11.4$ mag) becomes unity. The normalized flux in the Ks band is shown at the left side of Y axis and the radio flux at the right side. The light curves of the bright maser components and infrared emission show a similar trend but their date of the peak fluxes differs by dozens of days.

Table 1. Property of flux variations in the radio maser emission and the NIR continuum emission

	Maser (6.42 km/s)	Maser (5.83 km/s)	NIR (K_s)
MJD at peak flux	57339.5785	57317.6389	57368.5910
Flux at peak	1705 Jy	1632 Jy	8.0 mag
Flux at stable phase	0.5 Jy	60 Jy	11.4 mag
Decay timescale ¹	408 days	24 days	61 days
Magnification of flux ²	3400	27	23

1. timescale on that intensity decreases to half its peak.

2. flux magnification from its quiescent phase before burst event.

References

- Akitaya, H., Moritani, Y., Ui, T., et al. 2014, in Proc. SPIE, Vol. 9147, Ground-based and Airborne Instrumentation for Astronomy V, 914740
- Audard, M., Ábrahám, P., Dunham, M. M., et al. 2014, Protostars and Planets VI, 387
- Bartkiewicz, A., Szymczak, M., van Langevelde, H. J., Richards, A. M. S., & Pihlström, Y. M. 2009, A&A, 502, 155
- Boley, P. A., Linz, H., van Boekel, R., et al. 2013, A&A, 558, A24
- Burns, R. A., Handa, T., Nagayama, T., Sunada, K., & Omodaka, T. 2016, MNRAS, 460, 283
- Caratti o Garatti, A., Stecklum, B., Garcia Lopez, R., et al. 2017a, Nature Physics, 13, 276
- Caratti o Garatti, A., Cesaroni, R., Moscadelli, L., et al. 2017b, Mem. Soc. Astron. Italiana, 88, 773
- Cesaroni, R., Moscadelli, L., Neri, R., et al. 2018, A&A, 612, A103
- Cragg, D. M., Sobolev, A. M., & Godfrey, P. D. 2005, MNRAS, 360, 533
- Fujisawa, K., Yonekura, Y., Sugiyama, K., et al. 2015, The Astronomer's Telegram, 8286
- Hodapp, K. W., & Bressert, E. 2009, AJ, 137, 3501
- Howard, E. M., Pipher, J. L., & Forrest, W. J. 1997, ApJ, 481, 327
- Hunter, T. R., Brogan, C. L., MacLeod, G., et al. 2017, ApJ, 837, L29
- Kumar, M. S. N., Contreras Peña, C., Lucas, P. W., & Thompson, M. A. 2016, ApJ, 833, 24
- Meyer, D. M.-A., Vorobyov, E. I., Kuiper, R., & Kley, W. 2017, MNRAS, 464, L90
- Minier, V., Booth, R. S., & Conway, J. E. 2000, A&A, 362, 1093
- Morales-Calderón, M., Stauffer, J. R., Hillenbrand, L. A., et al. 2011, ApJ, 733, 50
- Moscadelli, L., Sanna, A., Goddi, C., et al. 2017, A&A, 600, L8
- Norris, R. P., Whiteoak, J. B., Caswell, J. L., Wieringa, M. H., & Gough, R. G. 1993, ApJ, 412, 222
- Ojha, D. K., Samal, M. R., Pandey, A. K., et al. 2011, ApJ, 738, 156
- Skrutskie, M. F., Cutri, R. M., Stiening, R., et al. 2006, AJ, 131, 1163
- Stecklum, B., Caratti o Garatti, A., Cardenas, M. C., et al. 2016, The Astronomer's Telegram, 8732
- Sugiyama, K., Fujisawa, K., Doi, A., et al. 2014, A&A, 562, A82
- Szymczak, M., Olech, M., Wolak, P., Gérard, E., & Bartkiewicz, A. 2018, A&A, 617, A80
- Tamura, M., Gatley, I., Joyce, R. R., et al. 1991, ApJ, 378, 611
- Tan, J. C., Beltrán, M. T., Caselli, P., et al. 2014, Protostars and Planets VI, 149
- Teixeira, G. D. C., Kumar, M. S. N., Smith, L., et al. 2018, A&A, 619, A41
- Zinnecker, H., & Yorke, H. W. 2007, ARA&A, 45, 481

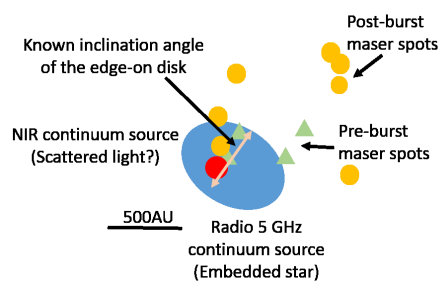


Fig. 4. Sky-plane image sketch of S255-NIRS3 region from radio observations including maser observations with VLBI (Moscadelli et al. 2017) and NIR observations (Stecklum et al. 2016). NIR and radio emitting region are separated by approximately 1 light days in the plane of sky, and this is considerably shorter than the observed delay between the radio and NIR flux peaks.

Appendix. Table of PSF fitting photometry results

Table 2. Results of PSF fitting photometry in the

<i>Ks</i> band		
MJD	S255-NIRS3 [mag]	Ref. star [mag]
57355.79	8.683 ± 0.023	10.908 ± 0.012
57356.77	8.692 ± 0.031	10.912 ± 0.024
57357.72	8.573 ± 0.033	10.883 ± 0.022
57360.51	8.315 ± 0.218	10.866 ± 0.061
57367.68	8.161 ± 0.070	10.649 ± 0.145
57368.59	8.030 ± 0.048	10.752 ± 0.178
57375.48	8.180 ± 0.085	10.862 ± 0.174
57378.48	8.176 ± 0.070	10.788 ± 0.105
57385.52	8.220 ± 0.030	10.757 ± 0.251
57393.57	8.343 ± 0.024	10.787 ± 0.117
57429.40	8.760 ± 0.083	10.832 ± 0.201
57441.55	8.844 ± 0.132	10.740 ± 0.130
57446.43	8.990 ± 0.059	10.817 ± 0.073
57450.52	9.148 ± 0.018	10.858 ± 0.024
57454.44	8.904 ± 0.007	10.864 ± 0.014
57487.45	9.356 ± 0.021	10.844 ± 0.015
57497.46	9.163 ± 0.004	10.820 ± 0.008
57738.62	10.401 ± 0.101	10.774 ± 0.231
57756.74	10.373 ± 0.020	10.867 ± 0.013
57770.45	10.299 ± 0.112	10.813 ± 0.035
57778.56	10.331 ± 0.076	10.679 ± 0.288
57797.65	10.534 ± 0.070	10.842 ± 0.014
57805.62	10.300 ± 0.014	10.837 ± 0.011
57813.49	10.420 ± 0.051	10.851 ± 0.015
58121.67	11.126 ± 0.154	10.824 ± 0.023
58569.44	11.747 ± 0.050	10.827 ± 0.026

Only relative magnitude errors are presented. There also exists systematic absolute magnitude of 0.1 mag.